Journal of Materials Processing Tech. 247 (2017) 243–256

Contents lists available at ScienceDirect

Journal of Materials Processing Tech.

journal homepage: www.elsevier.com/locate/jmatprotec

Investigation of post-weld rolling methods to reduce residual stress and distortion

Luis D. Cozzolino[a,*], Harry E. Coules[b], Paul A. Colegrove[a], Shuwen Wen[c]

[a] Cranfield University, Cranfield, Bedfordshire MK43 0AL, UK
[b] Department of Mechanical Engineering, University of Bristol, Bristol BS8 1TR, UK
[c] Tata Steel R, D & T, Swinden Technology Centre, Rotherham, South Yorkshire S60 3AR, UK

ARTICLE INFO

Keywords:
Residual stress management
Rolling
Welding
Modelling
FEA

ABSTRACT

The mechanisms of post-weld rolling and how it reduces and eliminates residual stress and distortion are poorly understood. Finite element analysis was applied to two different methods of rolling: rolling the weld bead directly with a single roller and rolling beside the weld bead with a dual flat roller. The models showed that both rolling techniques were able to induce compressive stress into the weld region, which increased with rolling load. The distribution of stress was sensitive to the coefficients of friction between the workpiece and the roller and the backing bar. High friction coefficients concentrated the plastic deformation and compressive stress within the centre of the weld bead. Distortion can be eliminated by rolling; however, the experiments indicated that this was only achieved when applied to the weld bead directly.

1. Introduction

Fusion welding involves uneven heating of the weldments, which causes a non-uniform temperature distribution and consequently local plastic strain in the weld and surrounding metal, as described in (Connor, 1987). The mismatch of the plastic strains between the weld and the parent metal causes residual stresses, which can have adverse effects on the mechanical properties and usually result in distortion.

To understand the generation of residual stress, computational weld mechanics can be used to simulate the large-scale effect of the heat source, as described by Lindgren (2007). Many simplifications may be adopted, which allow accurate results to be obtained in a relatively short time. Additionally, welding simulation can significantly reduce the number of experiments required to test particular design conditions to a few key ones for validating the models.

There are a number of residual stress mitigation techniques that can be used. Rolling is one that is effective, but has received relatively little attention in the literature. Kurkin and Tsyao (1962) analysed its beneficial effect in titanium alloys (OT4-1, VT-1, VT5-1), while Kurkin and Anufriev (1984) in aluminium alloys (Amg6 and 1201), obtaining significant residual stress reduction. Altenkirch et al. (2009) demonstrated its effectiveness for aluminium friction stir welds (FSW). In addition, numerical simulations conducted by Wen et al. (2010) in FSW, and Yang and Dong (2011) in low carbon steel TIG welds, have obtained results in agreement with the experimental findings. Recently, experiments conducted by Coules et al. (2013a, 2013b, 2012b) demonstrated how post-weld rolling can reduce distortion, and residual stress in Gas Metal Arc Welds (GMAW) in S355JR steel plates.

The process works by inducing positive local plastic strain in the welding direction, which counteracts the negative plastic strain generated during welding, as shown experimentally by Altenkirch et al. (2009), and the numerical models of Wen et al. (2010) for FSW, as well as by Yang et al. (1998) in TIG welds of aluminium alloy. Post-weld rolling is normally applied on top of the weld, by means of a single roller and is shown in Fig. 1(a). However, the technique can be applied with two rollers beside the weld bead which has been used to reduce the incidence of solidification cracking (Fig. 1(b)), as shown by Liu et al. (1996) in fusion welds of 2024-T4 aluminium alloy. Furthermore, fatigue cracks usually start from the weld toes, as shown by Tryfyakov et al. (1993). In this study deformation of the weld toes by ultrasonic impact peening treatment reduced the stress concentration caused by this region. In addition, McClung (2007) showed that tensile residual stress reduces the fatigue life of weldments. Therefore, post-weld rolling of the weld toes could potentially reduce these problems by reshaping the weld bead and inducing a compressive residual stress in the weld bead and surrounding metal.

In this paper, we describe the use of numerical models to predict the effect of post-weld rolling both on top of the weld bead using a grooved roller, and rolling beside the weld bead with a dual flat roller. The effects of parameters such as rolling load, roller position and width and

* Corresponding author.
E-mail address: daniel.cozzolino@outlook.com (L.D. Cozzolino).

http://dx.doi.org/10.1016/j.jmatprotec.2017.04.018
Received 26 August 2016; Received in revised form 20 April 2017; Accepted 23 April 2017
Available online 27 April 2017

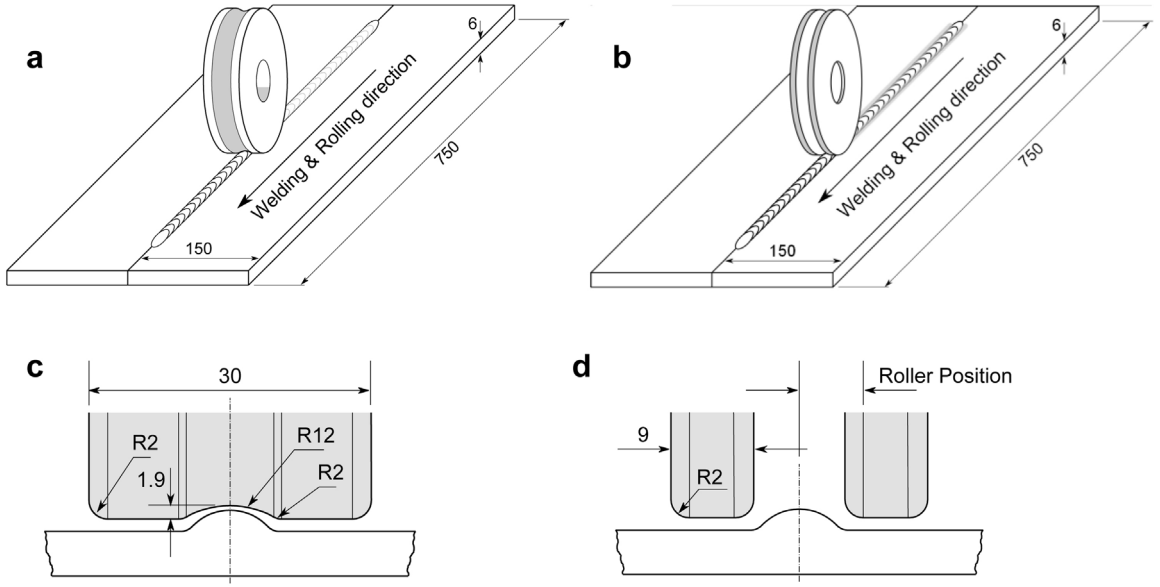

Fig. 1. Geometry and rolling methods for (a) rolling on top of the weld bead and (b) rolling beside the weld bead with the dual flat rollers; (c) roller dimensions used for rolling on top of the weld bead and (d) parameterised roller dimensions for rolling beside the weld bead (dimensions in mm).

their influence on the welding residual stress and distortion are determined and compared with equivalent experiments by Coules et al. (2013b). In addition, the influence of friction between the backing-bar, workpiece, and roller were also investigated.

2. Methodology

2.1. Numerical models

Linear single-pass bead-on-plate Gas Metal Arc Welds in rectangular plates of S355JR structural steel, and the subsequent rolling of these welds, were simulated using the finite element method. The models were run with Abaqus Standard version 6.9 as a sequentially coupled thermal-mechanical analysis. They consist of two main steps, namely a welding thermal-mechanical step to predict the welding-induced residual stress, and a rolling step to alter the residual stress formed from welding. A single set of welding parameters which are described in Section 2.2 were used for all the models.

2.1.1. Thermal model of the welding process

The models were three dimensional and simulate bead-on-plate welds on flat profile plates. Owing to the geometry of the experiments and to reduce computational time, only half of the geometry was modelled, which was also used for the subsequent rolling mechanical models. A typical mesh is shown in Fig. 2(a). A denser mesh was implemented on the weld bead region and on areas where rolling was subsequently applied. The effect of the mesh density was studied to ensure that the results presented are independent of the mesh size. The dimensions of half of the workpiece were 750 × 150 × 6 mm, and the weld seam was 600 mm in length. The average weld bead dimensions, measured by Coules et al. (2013a, 2013b, 2012b, 2012c) were Ø = 13.8, H = 2.9 and W = 5.6 mm.

The weld bead in these models was active during the entire welding step as well as the subsequent ones; hence the "dumped block" method, explained by Shan et al. (2007) was used and has sufficient accuracy for this work. Convective and thermal radiation heat losses were included from the top surface of the workpiece using a convective coefficient of 10 W m^{-2} $°C^{-1}$, as recommended by M. C. Smith and A. C. Smith (2009) for stainless steel bead-on-plate welds, and an emissivity of 0.8 was used as suggested by Simonson (1967). Even though the backing support was composed of both copper (underneath the weld bead) and aluminium in the far field, it was modelled with a temperature dependent convective heat transfer coefficient given by:

$$h(T) = ae^{bT} + c \tag{1}$$

where h is the convective heat transfer coefficient, and $a = 505.65$, $b = 158.89 \times 10^{-5}$, and $c = -400$ are constants which were determined by trial and error. The welding heat, q was applied in all the models with a double ellipsoid volumetric heat source distribution proposed by Goldak et al. (1984):

$$q = \frac{6\sqrt{3} f_f Q}{a_f bc\pi\sqrt{\pi}} e^{-3x^2/a_f^2} e^{-3y^2/b^2} e^{-3z^2/c^2} \quad ifx \geq 0$$
$$q = \frac{6\sqrt{3} f_r Q}{a_r bc\pi\sqrt{\pi}} e^{-3x^2/a_r^2} e^{-3y^2/b^2} e^{-3z^2/c^2} \quad ifx < 0 \tag{2}$$

where a_f, a_r, b, and c are geometrical factors for the ellipsoidal shape; x, y, and z are the coordinates of the geometry, f_f and f_r are the heat input fraction in the front and rear ellipsoid quadrants, and their summation must equal two. Finally, Q is the welding power.

Since the weld bead was entirely present during the welding step, the double ellipsoid heat input was centred on the top of it, as shown in Fig. 3. Owing to the mismatch between the weld bead and double ellipsoid shapes, not all the heat in the double ellipsoid was actually applied to the weldment. The geometrical parameter of the double ellipsoid were considered initially as 90% of the molten region observed in the experiment, as proposed by Goldak and Akhlaghi (2005); however this approach did not produce a good match with the temperature profiles obtained in the experiments. Therefore, these parameters (*af*, *ar*, *b*, *c*) were tuned manually until a good match with the temperature profile was obtained. The final values were smaller than 90% of the weldpool dimensions.

In Table 1 the parameters for the Goldak double ellipsoid heat source are reported.

Temperature dependent thermal properties used are reported in Fig. 4 (Thompson et al., 2008). Michaleris and Debiccari (1997) sugested to artificially increase the thermal conductivity above the melting point to take into account the stirring effect present in the weld pool. The latent heat of fusion, 272 kJ kg^{-1} K (Al-Sulaiman et al., 2007), and of vaporisation, 6258 kJ kg^{-1} K (Al-Sulaiman et al., 2007), were included in the analysis between 1500 and 1530 °C, and 3090 and 3100, respectively.

After the heat induced by the welding process was finished, an additional 600 s cooling step was applied to allow the weldment to cool

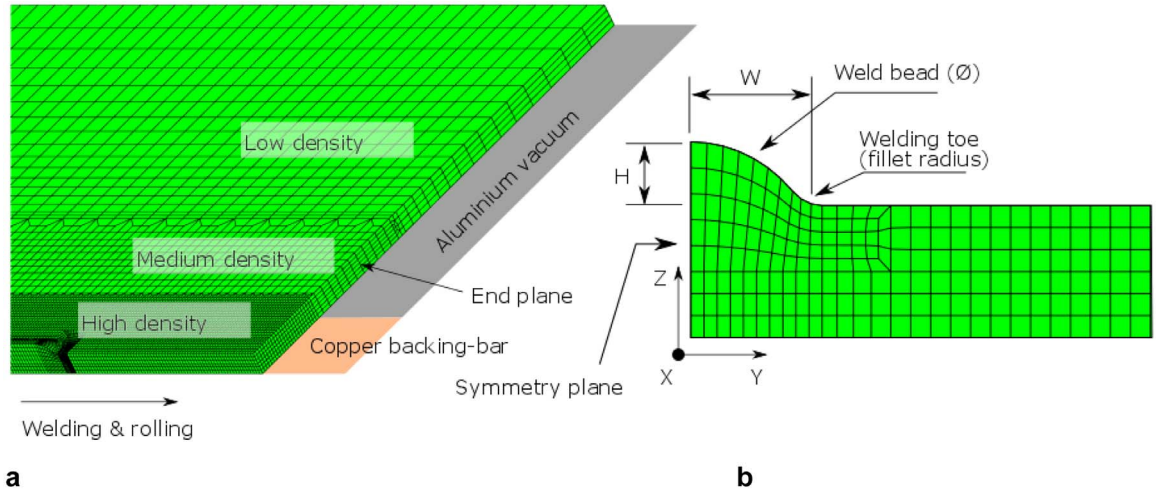

Fig. 2. (a) Example of different mesh densities through the plate width; and (b) weld-bead profile.

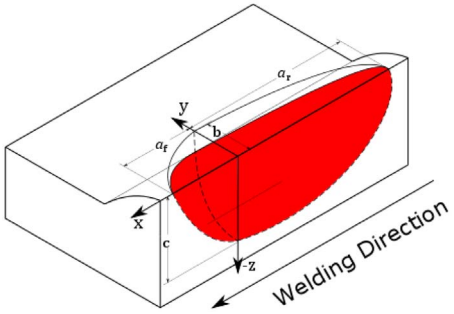

Fig. 3. Isometric view of the heat source which shows how it was applied to the weld bead profile.

Table 1
Parameters for the heat source.

Double ellipsoid parameters					
Welding speed [mm min^{-1}]	a_f [mm]	a_r [mm]	b [mm]	c [mm]	Q [W]
500	9.0	2.0	3.0	6.7	12096

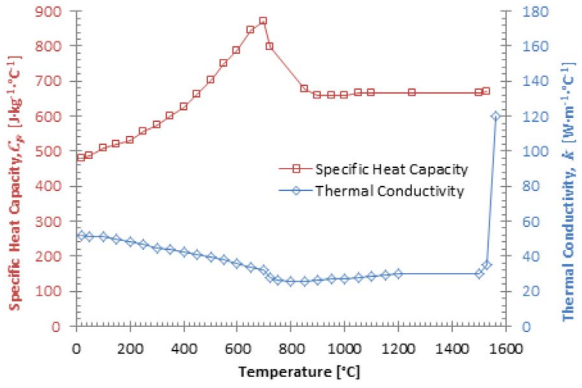

Fig. 4. Temperature dependent material properties used for the model.

to room temperature (about 20 °C).

The models were run on a High Performance Computer (HPC) with 80 nodes; each node had two Intel E5-2660 (Sandy Bridge) CPUs with 16 cores for each CPU. The thermal model used 64 nodes and took 10.2 h to solve.

2.1.2. Mechanical model of the welding process

In these models, the transient stress due to the welding thermal history as predicted in the previous thermal modelling step was investigated. Linear elements with reduced integration were used since they reduced the solution time compared to quadratic ones (Dessault Systemes, 2009). Temperature dependent mechanical properties for mild steel S355 (Shown in Fig. 5) were used in all models; which were supplied by Tata Steel Research Development and Technology, Swinden Technology Centre (Thompson et al., 2008). Directionally isotropic elastic-plastic mechanical properties were assumed. The linear thermal expansion coefficient used in the analyses, shown in Fig. 5(a), is the average value of different cooling rates from 429 to 0.4 °C s^{-1}, which represent average welding conditions. The volume change that occurs due to the phase change from austenite to ferrite was indirectly included through the variability in the thermal expansion coefficient that occurred around the transformation temperature (Fig. 5(a)). Annealing of the material, which eliminated the plastic strain history due to isotropic hardening was included for temperatures above 950 °C. This value was chosen because work hardening of the material above this temperature was negligible.

To generate the stress due to welding, the nodal temperature history obtained from the welding heat transfer analysis, described in the previous section, was imported into the welding mechanical model. This caused the expansion and contraction of the material and plastic deformation occurred where the yield criterion was exceeded.

Since only half the geometry was modelled, a symmetric boundary condition was applied to the symmetry plane (see Fig. 2(b)). To simulate the vacuum clamping system the displacement in the out-of--plane direction of all the nodes on the lower surface was restrained. To avoid the displacement in the longitudinal direction, all the nodes on the end plane (see Fig. 2(a)) of the weldment were restrained.

After welding and cooling to room temperature, an extra step was added to simulate unclamping. In this step, one node in the middle length of the symmetry plane was fully restrained in all degrees of freedom (encastré). At the same time all the other mechanical constraints were released, except for the ones on the symmetry plane, allowing the workpiece to deform, and some of the residual stress to relax as happens in reality.

2.1.3. Mechanical model of the rolling process

The results of the weld mechanical model were used as the input for the mechanical rolling models. The rollers and backing support were modelled as rigid shell bodies and were therefore not deformable. Unlike the welding thermal-mechanical steps, the vacuum clamps were modelled by applying one atmosphere pressure (101325 Pa) on the lower surface of the workpiece towards the backing support. In

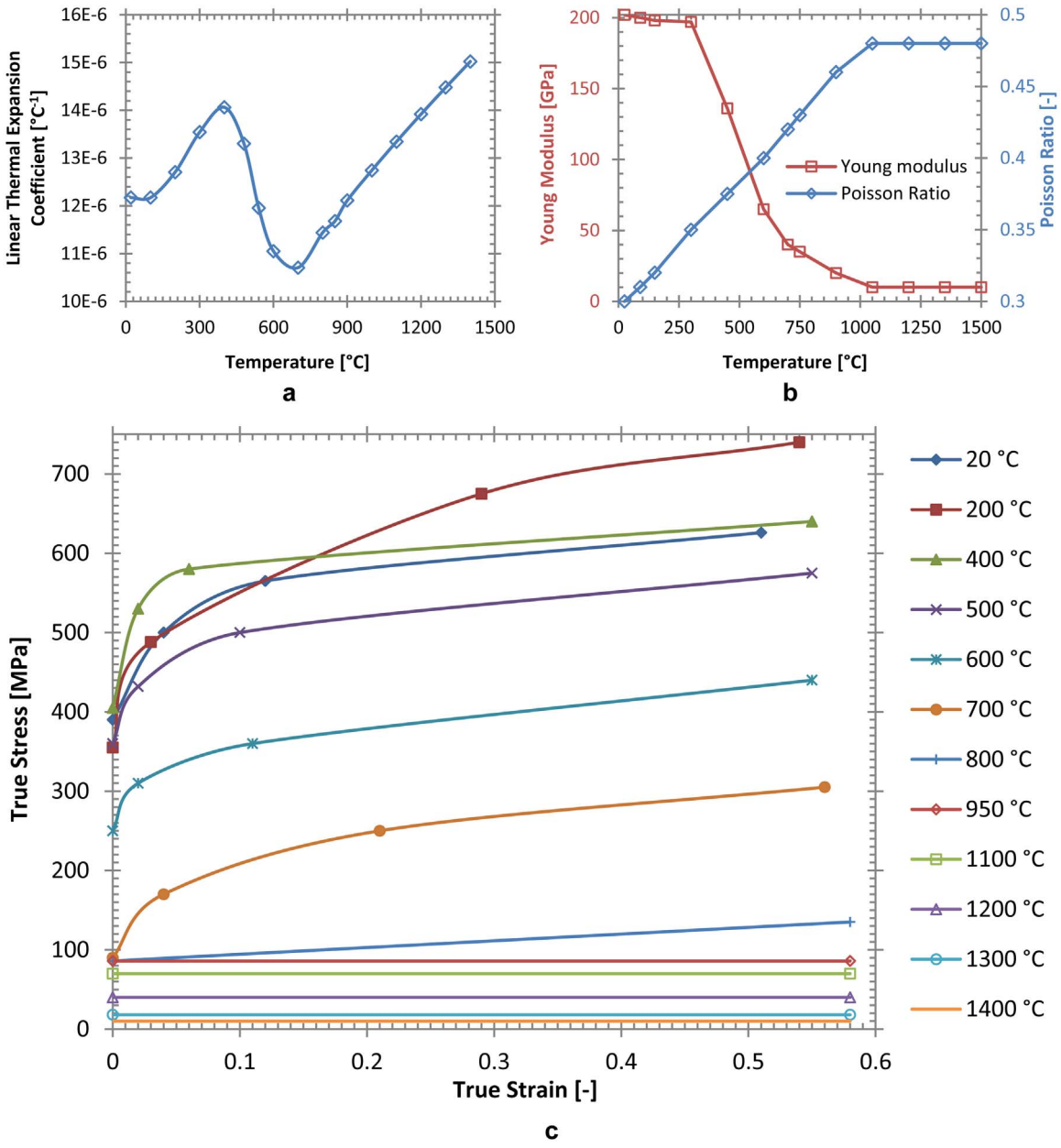

Fig. 5. Mechanical properties of S355: (a) Linear thermal expansion coefficient; (b) Young's modulus and Poisson ratio; and (c) True stress vs. true plastic strain curves (Thompson et al., 2008).

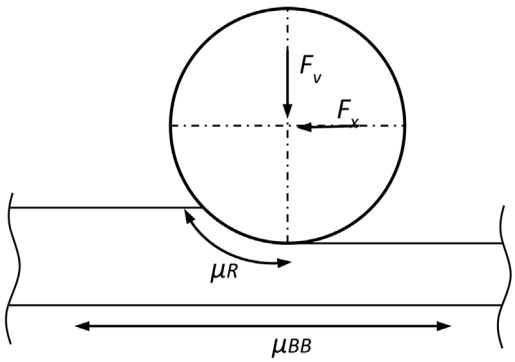

Fig. 6. Rolling boundary conditions, where: *Fy* is the vertical force, *Fx* is horizontal force (at constant horizontal speed), μR is the friction coefficient between the roller and a the workpleace and the μBB is the friction coefficient between the workpiece and the backing bar.

addition, to simulate the friction interaction of the backing-bar and the workpiece, different isotropic constant friction coefficients were considered. These were applied in a strip of 48 mm width in the middle of the workpiece (24 mm in half model), along its lower surface. The remaining area in the bottom plane was considered frictionless. All the rolling steps used the same rolling speed, 500 mm min^{-1}, and no torque was applied to the roller to induce the roller translation (free rolling), the rolling boundary conditions are shown in Fig. 6. After rolling, an unclamping step was performed to determine distortion using the procedure described in Section 2.1.2.

Two types of rollers were investigated; namely, single grooved, and dual flat rollers, as shown in Fig. 1. The single grooved roller consisted of a 100 mm external diameter roller with a groove radius, as shown in Fig. 1(c), which was used to roll the top of the weld bead. The groove radius (12 mm) was larger than the effective mean weld bead radius (6.9 mm measured by Coules et al. (2013a, 2013b, 2012b, 2012c)). The dual flat rollers are composed of twin rollers which rolled both sides of the weld bead simultaneously, as shown in Fig. 1(d). These rollers had

Table 2
Parameters investigated when rolling on top of the weld bead.

Rolling Load [kN]	Friction Coefficient Backing-bar − Plate, μ_{BB} [–]	Friction Coefficient Roller − Plate, μ_R [–]
25	0.0; 0.5	0.0
25	0.2	0.5
50	0.2	0.5
100	0.2	0.5
150	0.0; 0.2; 0.5; 1.0	0.0
150	0.2	0.2; 0.3; 0.5
150	0.5	0.2; 0.3; 0.5; 0.8

2 mm fillet radius at their corners, were 9 mm wide and had a diameter of 100 mm. The transverse positioning of the roller, as it is defined in the analysis, is shown in Fig. 1(d).

A set of models using the single-roller process was used to investigate the effect of different friction coefficients between the backing-bar and the workpiece, and between the roller and the workpiece, as well as the effect of different rolling loads in the residual stress distribution. The parameters explored are reported in Table 2.

For dual rolling, two sub-sets of models were investigated and are summarised in Table 3. The first sub-set analysed the influence of different dual roller transverse distances, from 6.5 mm, in which there was virtually no contact between the rollers and the weld bead, to 6 mm in which not only were the welding toes rolled, but the weld bead was significantly deformed too. A smaller model of 456 × 150 × 6 mm which had a weld bead length of 408 mm and a rolled length of 120 mm was used to reduce the computational time. Friction coefficients of 0.5 between the backing-bar and the workpiece and 0 elsewhere were used. A study was done to show that the results from this reduced size workpiece were approximately equivalent to the larger size workpiece. The second sub-set used a friction coefficient of 0.2 with the backing-bar and 0.5 with the roller and was used for comparison with experimental results.

All the rolling models were run on the HPC described earlier, using a different number of computational cores (32–60 cores), with a computational time that increased when the rolling load increased, and when the friction coefficient was applied. The wallclock time varied from 32.9 h with a low load and no friction to 95.3 h with large loads and friction. The models showed some convergence issues when the mesh was coarse in the contact region between the roller and the workpiece. Increasing the density of the mesh of the workpiece in those regions solved those issues.

2.2. Experimental

Experiments were performed to determine the effect of rolling on the residual stress distribution in welds under the various different rolling conditions considered in the modelling investigation. 6 mm plate specimens of EN100025:2004 S355JR structural steel with the dimensions as described in Section 2.1.1 were welded down their centreline and then rolled using different rolling techniques. Pulsed-current Gas Metal Arc Welding (GMAW) with a single set of welding parameters which are listed in Table 4, and are described in detail by Coules et al. (2013b, 2012b), was used throughout the experimental work. Note that the power input was determined from a AMV 4000 welding monitor (Triton Electronics Ltd.) arc monitoring device. The thermal model described in Section 2.1.1 was designed to represent this particular welding process. Rolling was performed using a hydraulic rolling machine described by Coules (2012). 3D laser coordinate scans were taken of all the specimens involved using a Romer Omega-arm with an R-Scan laser scanning head. This allowed the welding-induced distortion of the plates to be quantified and compared with the modelling results (see Fig. 12).

Table 3
Parameters investigated with the dual roller beside the weld bead.

Model Sub-Set	Rolling Load [kN]	Roller Position [mm]	Plate size L × W × T [mm]	μ_{BB} [–]	μ_R [–]
Sub-Set 1	50	6; 6.1; 6.3; 6.5	456 × 150 × 6	0.5	0
	75	6; 6.2; 6.5	456 × 150 × 6	0.5	0
Sub-Set 2 (Validation)	25; 50; 100; 150	6	750 × 150 × 6	0.2	0.5

Table 4
Parameters used for welding trials.

Parameter	Value
Power supply	Fronius TransPuls Synergic 5000
Synergic Mode	Pulsed-spray
Welding speed [mm min^{-1}]	500
Wire feed speed [m min^{-1}]	15
Filler wire	ISO 14341-A-G3Si1, 1.0 mm dia.
Shielding gas	20% CO_2, 2% O_2, balance Ar
Shielding gas rate [l min^{-1}]	10
Mean current [A]	328
Mean voltage [V]	35.1

The residual stress distribution within each rolled weld specimen was measured using neutron diffraction. Two separate neutron diffraction investigations were performed. The first investigation considered welds rolled on the top of the weld bead with different rolling loads (Coules et al., 2012b). Measurements on this set of specimens were performed using the SALSA neutron diffractometer (Institut Laue-Langevin, Grenoble, France) and the results are shown in Fig. 10. The second investigation considered welds rolled using different roller profiles (Coules et al., 2013b). The neutron diffraction measurements for this investigation were performed using the ENGIN-X instrument (ISIS facility, Rutherford Appleton Laboratory, UK) and the results are shown in Figs. 11a and 14a. Details of all the measurements involved are given in Coules thesis (2012).

3. Results and discussion

3.1. Welding heat transfer model

The position of the thermocouples in the experiments conducted by Coules et al. experiments (2012b) is shown in Fig. 7a. Comparisons between the experimental and predicted temperature distribution of the welding heat transfer analysis of the post weld models is shown in Fig. 7b. the model showed very good agreement with the experimental results.

3.2. Rolling on top of the weld bead

3.2.1. Modelling results

Fig. 8 shows the longitudinal residual stress at the mid-thickness transverse to the weld direction, after rolling on top of the weld bead with the 25 kn rolling load, and different friction coefficients. This illustrates how the coefficient of friction has negligible effect on the residual stress where the rolling load was low. When applying a higher load of 150 kn, the coefficients of friction had a much more significant effect which is shown in Fig. 9.

The effect of friction on deformation during compression testing was analysed by Cook and Larke (1945), which has similarities to the rolling process studied in this work. These authors found that the presence of friction restrained the material in the contact area (tool for compression testing and roller in our case), reducing the plastic strain at the surface.

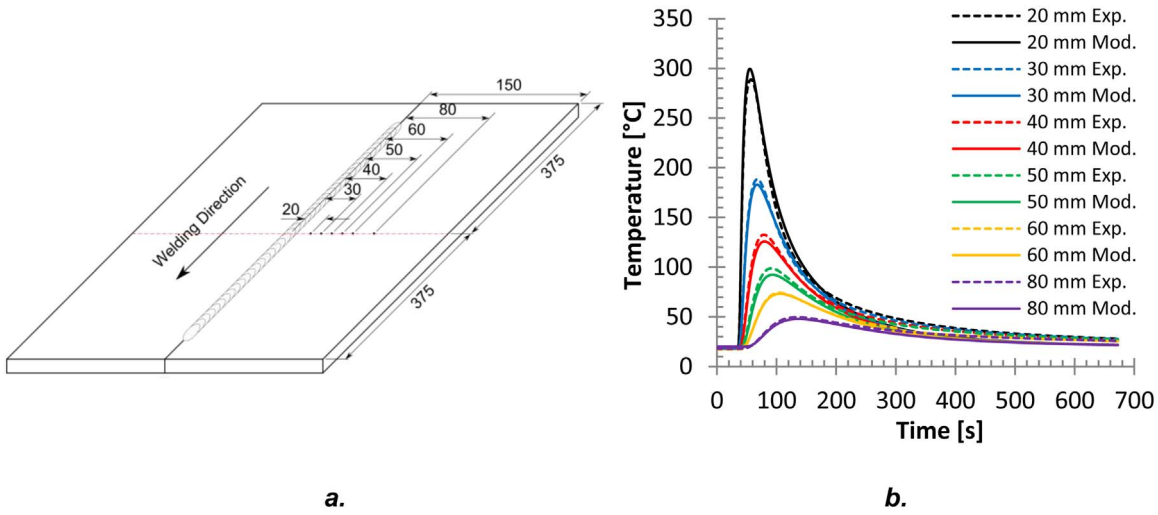

Fig. 7. *a.* Position of the thermocouples on post-weld rolling experiments (Coules et al., 2012b) (dimensions in millimetres). *b.* Comparison between experiments (Exp) and modelling results.

For low loads, where the deformation is small there was very little effect of the friction coefficient. However, as the load increased, more deformation occurred *within* the material relative to the surface where there was a high friction coefficient. This resulted in a significant difference in the residual stress distribution compared to the frictionless condition.

The different coefficients of friction caused a significant difference not only with the magnitude of the residual stress but also its distribution with the 150 kn rolling load. In the complete frictionless model (Fig. 9(a)), most of the compressive residual stress was localised close to the lower surface. Adding friction to the backing-bar (especially Fig. 9(c)), restrained the lower surface and caused more plastic deformation within the material which resulted in the region with a peak compressive residual stress shifting to the middle of the weld. Increasing the friction coefficient on the roller concentrated the compressive region in the middle of the weld bead. Hence low friction coefficient conditions produce a more uniform stress distribution through the thickness which could be beneficial for performance – particularly fatigue. The plastic strain that occurred within the material for a particular set of friction coefficients (0.2 with the backing-bar and 0.5 with the roller) is shown in Fig. 10. This demonstrates how the plastic strain is concentrated in the middle of the weld bead in the longitudinal direction (Fig. 10(a,b)). In the transverse and normal directions the peak is located closer to the top of the weld bead (Fig. 10(c,d)). There is a significant change in the bead profile near the top surface (see Fig. 11) which causes strains and stresses in the lateral and normal directions in this same region.

One of the interesting consequences of the concentration of the plastic deformation within the centre of the weld bead is that tensile stresses are generated on top of the weld bead, which balance the compressive stresses generated in the weld centre. This phenomenon has been reported previously by Bijak-Zochowski and Marek (1997) who studied the influence of rolling on steel strips. The results indicated that the tensile stresses were greatest with a friction coefficient of 0.2 with the roller. It is not clear why the tensile stresses were greater with this condition than for a friction coefficient of 0.8.

Fig. 11 shows the longitudinal component of residual stress after rolling the top of the weld bead, with 25, 50, 100, and 150 kn. The friction coefficient between the backing-bar and the weldment was 0.2, and between the roller and the weldment was 0.5. Half of the roller was added to the contour plots, to show how the contact sections and the weld bead shapes changed with the rolling load. When rolling the top of the weld bead, the material in contact with the roller tends to be deformed in all the directions, but it is restrained by the roller shape and the tangential forces derived from the frictional contact. With low loads, the deformation is limited to the very top of the weld bead, as shown in Fig. 11(a), and the transverse plastic deformation is restrained mainly by the small frictional contact region. A large compressive

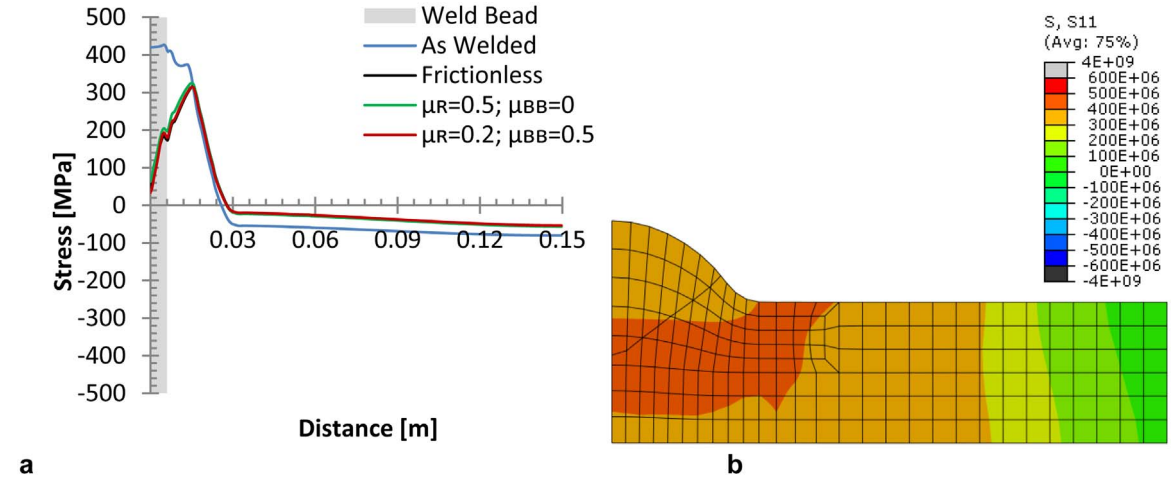

Fig. 8. (a) Mid-thickness longitudinal residual stress after rolling on top of the weld bead using 25 kn load and different friction coefficients between the workpiece and the backing bar (μ_{BB}), and the roller (μ_R); and (b) contour plot of longitudinal residual stress in the mid-length transverse cross section after welding.

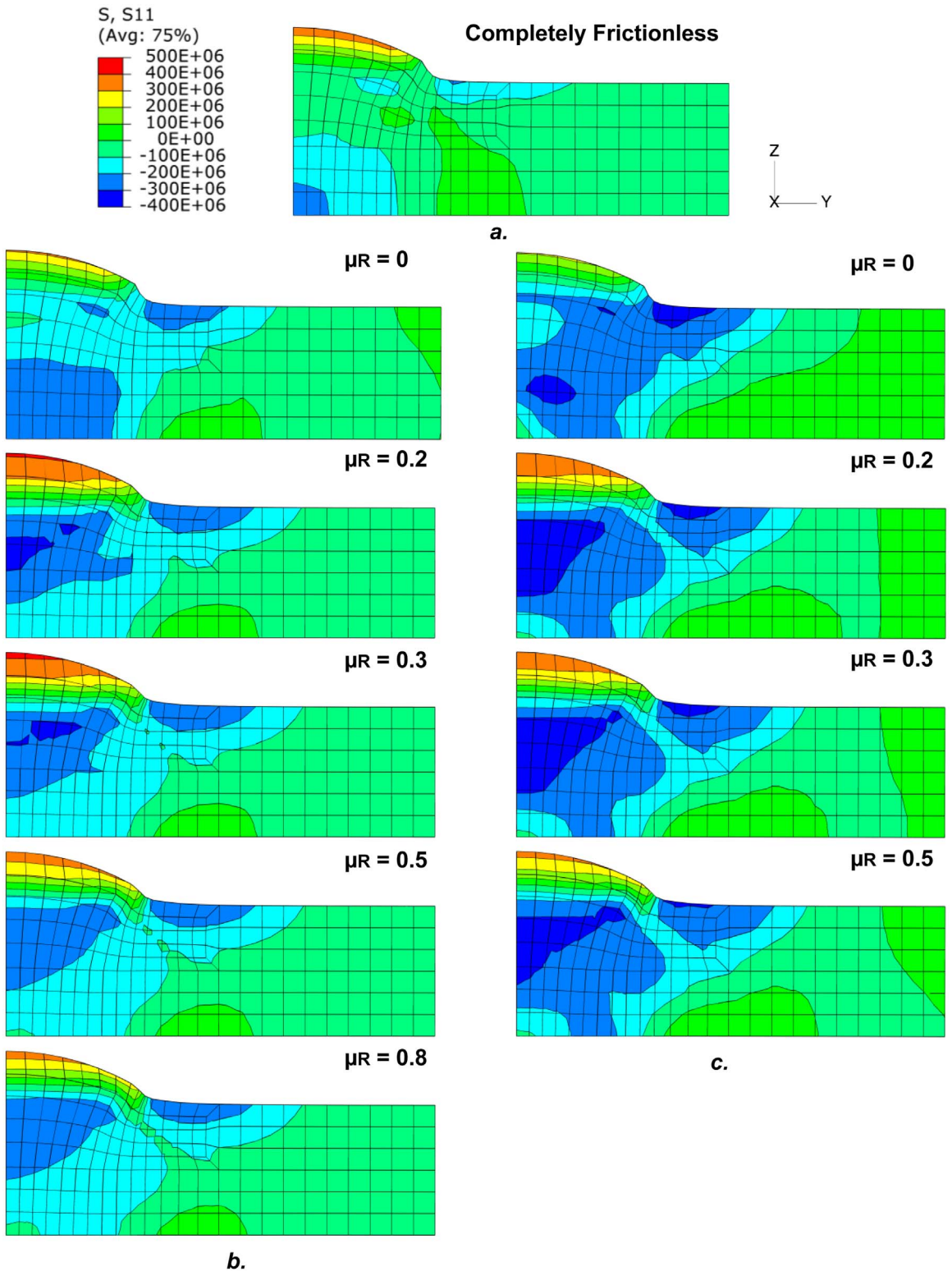

Fig. 9. Contour plot of the longitudinal residual stress within 20 mm from the weld centreline, rolled with a 150 kn load, with different friction coefficient between workpiece and backing-bar (μ_{BB}); (a) frictionless, and (b) μ_{BB} = 0.2, and (c) μ_{BB} = 0.5, with different friction coefficients between the roller and workpiece (μ_R).

longitudinal residual stress is formed in the weld bead next to the welding toes, and a few millimetres underneath the contact region. With large loads, the weld bead deformation is greater, substantially increasing the contact between the roller and weld bead, whilst the weld bead adopts the shape of the roller groove. Consequently, larger frictional tangent forces are produced, increasing the compressive stress in the weld bead core, as shown in Fig. 11(d).

3.2.2. Experimental validation

The best match between the models and the experimental results were obtained by using a friction coefficient between the backing-bar and the weldment of 0.2, and between the roller and the weldment of 0.5. One possible reason why the coefficient of friction with the roller was higher than with the backing bar is the higher roughness of the weld bead – compared to the interface between the backing bar and

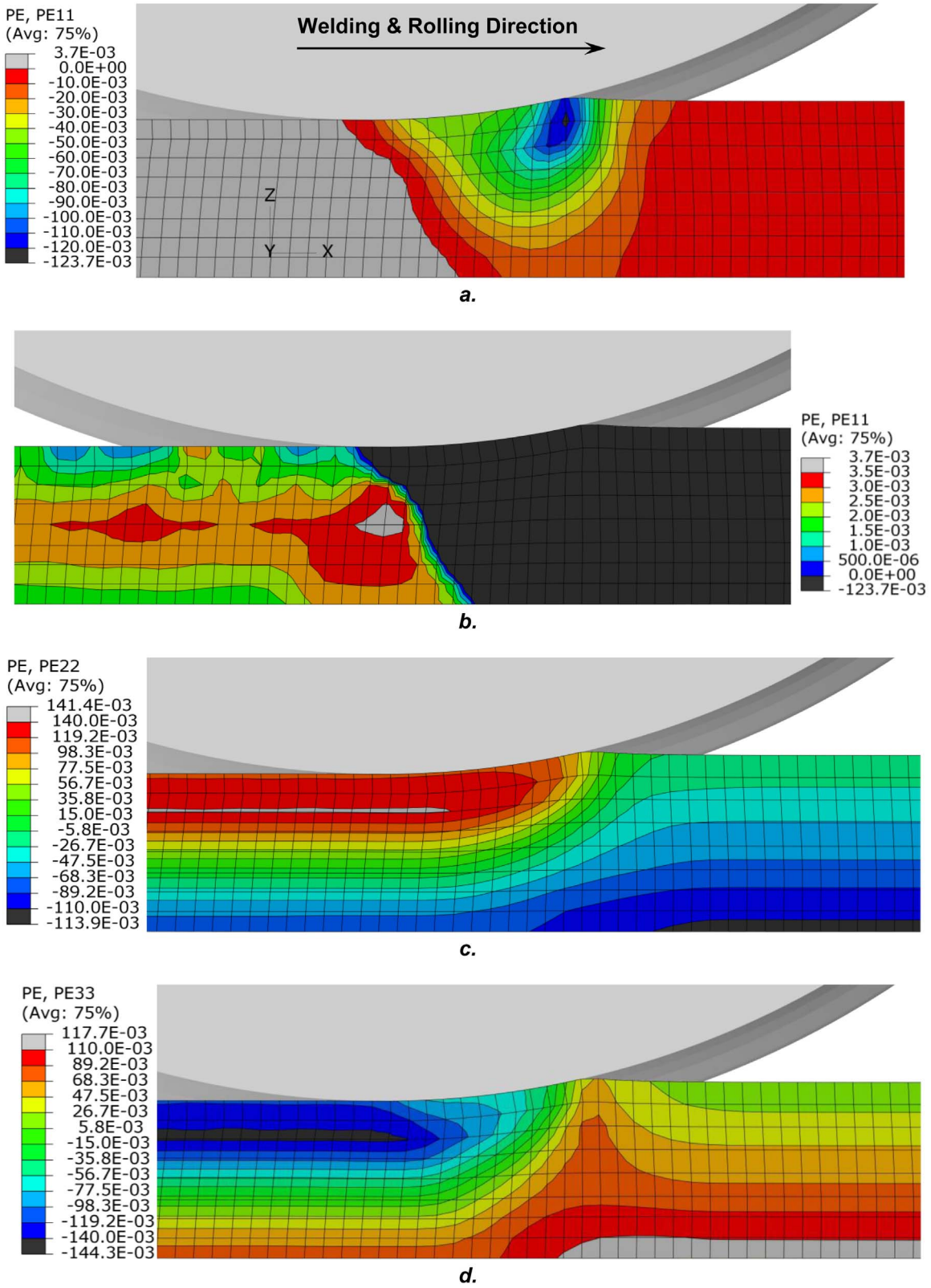

Fig. 10. Contour plots of the predicted plastic strain with a friction coefficient of 0.2 with the backing-bar and 0.5 with the roller, and a load of 150 kn; (a) compressive, and (b) tensile in the longitudinal direction, and (c) transverse, and (d) normal directions.

workpiece. Fig. 12 shows a comparison of the longitudinal residual stress between the experiments and numerical models for this condition. The longitudinal tensile peak of the residual stress is reduced by rolling, and as the load increases, the longitudinal tensile residual stress decreases and the region affected by the roller is widened.

Although the results are largely in agreement, there are some small discrepancies, particularly in regions where the stress gradient is large. In the experiments a gauge volume of $2 \times 2 \times 2$ mm was used by Coules et al. (2012b) (which is shown in Fig. 11) which averages the stresses within that volume. As stated in Price et al. (2008) this can

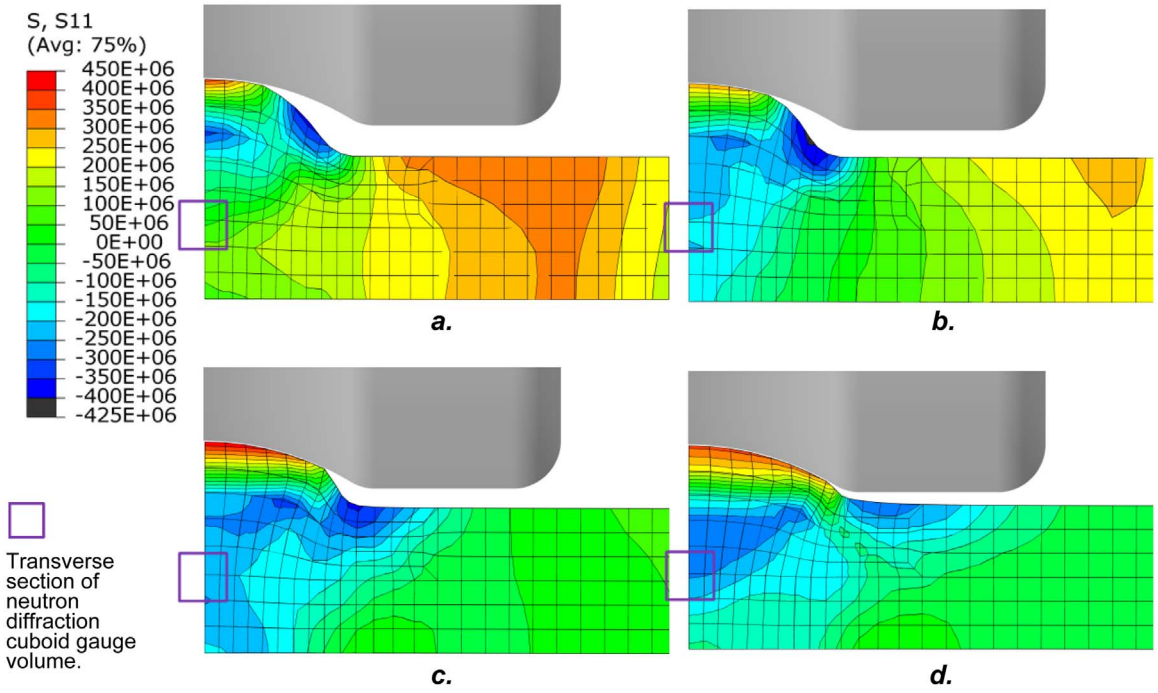

Fig. 11. Contour plot of the longitudinal residual stresses, within 20 mm from the weld centreline, after rolling with: *a.* 25; *b.* 50; *c.* 100; and *d.* 150 kn. μBB = 0.2 and μR = 0.5.

cause a discrepancy with the model results which are determined at a point.

Fig. 13 shows experimental and predicted contour maps of the longitudinal residual stress after rolling with a load of 150 kn. The modelling results were cropped to the same size as the experiments to aid interpretation. The cross marks in the experimental contour plot represent the actual neutron diffraction measurements. There is reasonable agreement in the weld region with tensile stresses near the top surface and compressive stresses being generated in the centre of the weld. The agreement around the weld toes and HAZ was poorer – the experiment had a strongly tensile stress towards the upper surface while the results for the numerical model were opposite.

Fig. 14(a) shows the distortion obtained for different rolling loads and Fig. 14(b) shows a comparison of the out-of-plane distortion for the experimental and numerical results. Both the experiments and the numerical model predict that there is a significant amount of distortion in the as-welded condition which is reduced to negligible values by rolling. The rolling load had minimal impact on the amount of distortion – negligible distortion was obtained even with a load of 12.5 kn. There was a reasonable amount of variation in distortion between nominally identical experimental specimens (Coules et al., 2012a). In addition, the plates were not completely flat prior to welding (unlike the numerical model) which may also impact the final out-of-plane distortion.

The distorted shape of the as-welded condition for both the predicted and experiment resembled a hyperbolic paraboloid (saddle shape), being concave, and its out-of-plane peaks were 6.30, and 9.89 mm, respectively. In this study, this kind of distortion was considered negative. The predicted distortion after rolling was in the opposite direction (convex) for all the rolling loads analysed, and this type of distortion was considered positive.

The plate distortion is mainly due to bending. The presence of the weld bead and the non-uniform tensile residual stress through the thickness in the weld bead region displaces the neutral axis of the workpiece above the mid-thickness of the plate. When the workpiece is unclamped the residual stress redistributes causing a bending moment which distorts the weldment. Rolling on top of the weld bead induces a tensile plastic strain and a compressive residual stress predominantly in the upper part of the workpiece thickness; therefore, when the weldment is unclamped it deforms in the opposite direction to the as-welded sample.

3.3. Rolling the weld toes

3.3.1. Modelling results

Fig. 15 shows the longitudinal residual stress, after rolling the welding toes with the dual flat roller, at different roller positions and 50 and 75 kn load. The roller did not touch the weld toes at a position of 7 mm.

All cases analysed in this section generated large reductions in the longitudinal tensile residual stress peak and width. The dual flat roller caused longitudinal compressive residual stress regions along its path (at each side of the weld bead). In the weld bead region, the longitudinal welding residual stress was significantly reduced, while on the other sides of the rolling paths, in the parent metal, the longitudinal tensile residual stress was increased from the as-welded original distribution. The 75 kn load caused a larger reduction of the tensile peak at the centreline, and a larger reduction of the tensile residual stress peak width, than the 50 kn one.

At 6 mm from the centreline the longitudinal residual stress in the weld bead region was compressive with both, 50 and 75 kn rolling loads, as shown in Fig. 15. Increasing this distance reduced the compressive residual stress induced by rolling, and at 6.5 mm the longitudinal residual stress was tensile in the weld bead. When the roller was positioned 7 mm from the weld centreline, the residual stress reduction at the centreline was minimal. This is because the roller “squeezes” the weld metal between the two inner sides of the roller with the smaller distances, producing more deformation of the weld metal which reduces the longitudinal residual stress. Consequently, physical variations in the weld bead width would yield varying longitudinal residual stress regions along the weld, as well as out-of-plane distortion.

3.3.2. Experimental validation

Fig. 16 shows a comparison between the experimental and predicted longitudinal residual stress, after rolling with a load of 150 kn in the

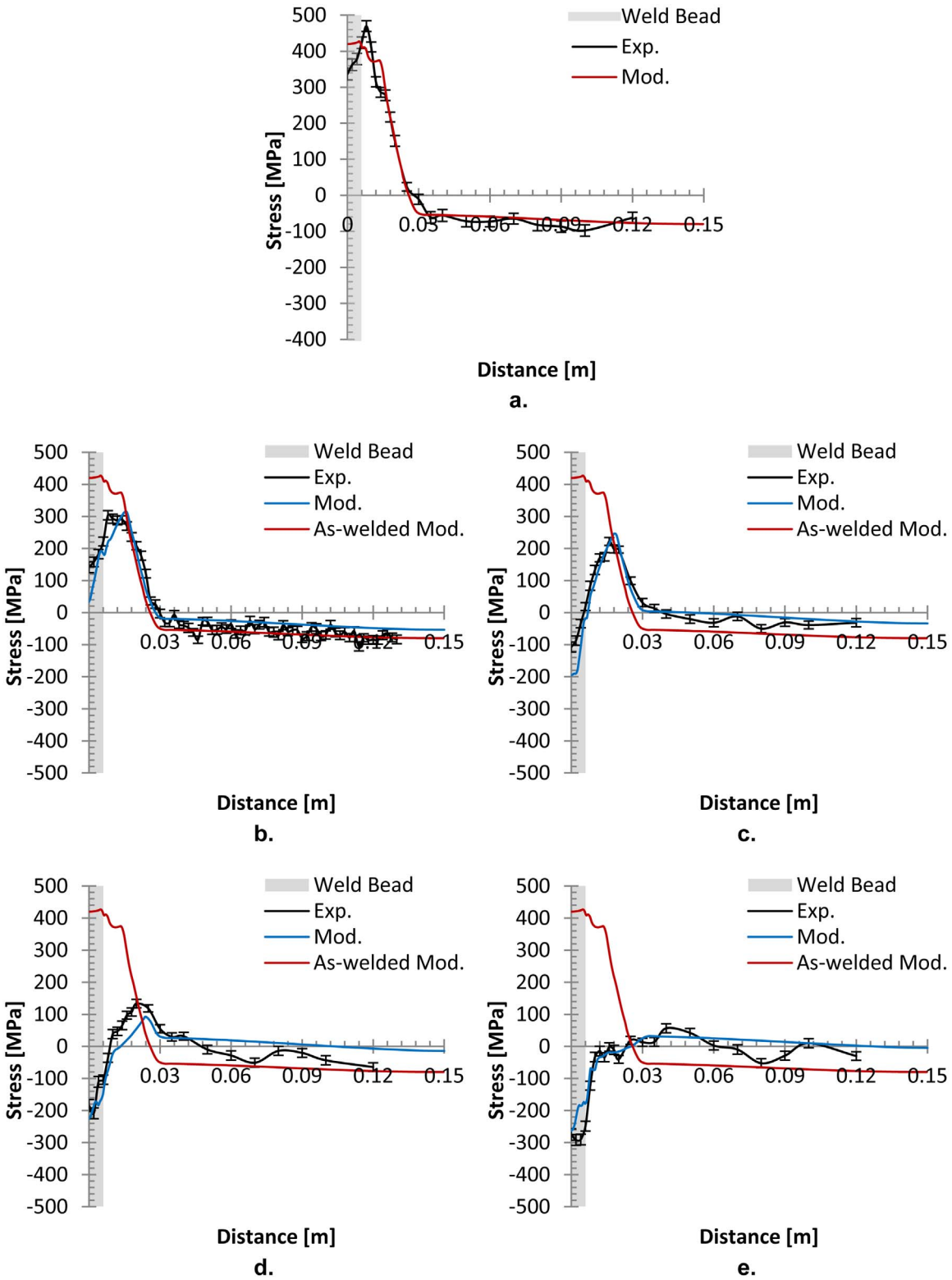

Fig. 12. Mid-thickness longitudinal residual stresses vs. transverse distance to the weld direction. Comparison between modelled and experimental results after rolling on top of the weld bead with: (a) as-welded; (b) 25; (c) 50; (d) 100; and (e) 150 kn loads.

weld direction, within 20 mm from the weld centreline. The longitudinal residual stress had discrepancies mainly in the first 10 mm from the weld centreline. Further away, the predicted longitudinal residual stress shows better agreement with the experiments. The experiments showed a slightly tensile region in the weld bead zone, while the predicted results showed a very compressive residual stress in the same region. Below the region rolled (indicated by the red line) the experiments showed a compressive region close to the upper surface, whereas in the model, the compressive region was more uniform through the thickness. On the other hand, in the parent metal the residual stress of both, experiment and model, was between ± 50 MPa.

The discrepancies in the longitudinal residual stress between the experiment and model, could in part be due to the weld bead width variation along the weld seam. As shown previously in Fig. 15 the

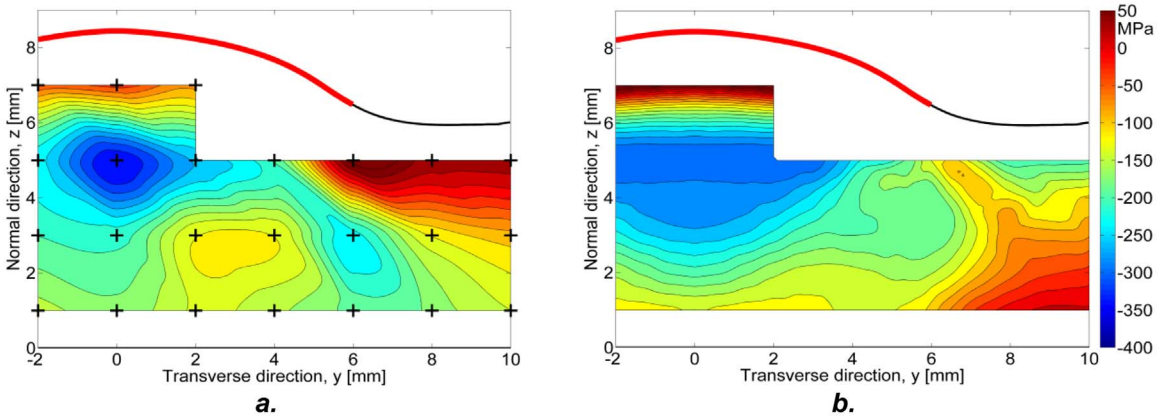

Fig. 13. Contour plots of longitudinal residual stress in the weld bead sections after rolling with a 150 kn load; (a) experimental measurements (Coules et al., 2013b), and (b) modelling results.

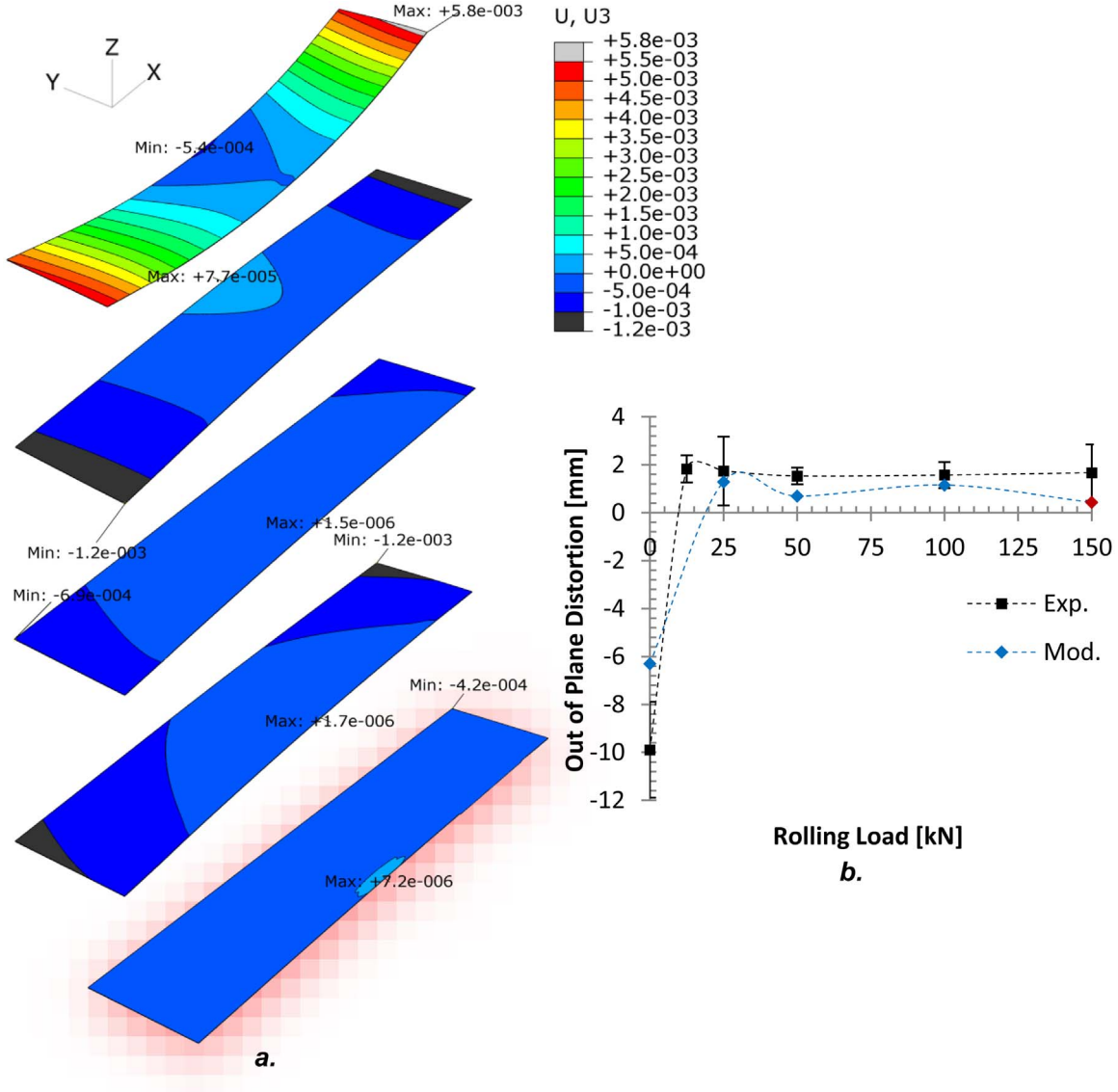

Fig. 14. (a) Contour plot of out of plate distortion after rolling the top of the weld beads, with different loads; from top to bottom: 0 (as-welded), 25, 50, 100, and 150 kn. (b) Out-of-plane distortion vs. rolling load.

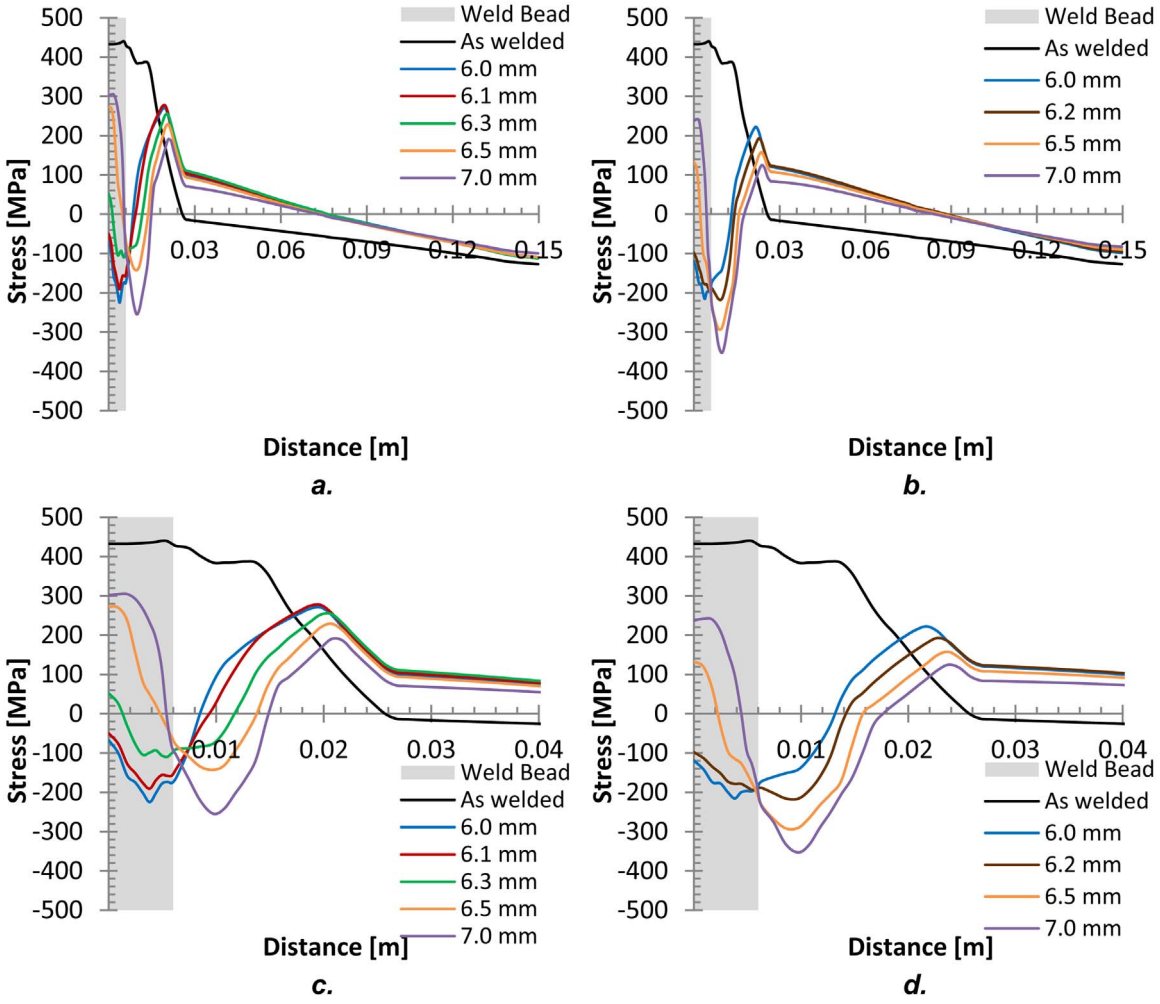

Fig. 15. Longitudinal residual stress after rolling on the welding toes, at different roller positions relative to the weld for rolling loads of (a) 50, and (b) 75 kn; and a close-up of the first 40 mm from the welding centreline with (c) 50, and (d) 75 kn.

residual stress reduction is critically dependent on the roller position relative to the weld toe which may explain the differences with the experimental observations. Although, the longitudinal residual stress reduction was overestimated by the model, it showed that rolling the weld toes caused a large reduction to the longitudinal residual stress which was also observed in the experiment.

Fig. 17 shows the predicted and measured out-of-plane distortion after rolling the weld toes. There was a significant discrepancy between the two values with the distortion being eliminated in the model, and it was only reduced slightly compared to the as-welded condition in the experiments. The location of the roller and its effect on the residual stress could be one cause. The evidence presented here indicates that there is no benefit in reducing distortion by rolling beside the weld bead as compared to rolling directly on top of it. Furthermore, Coules et al. (2013b) have shown previously that this process can reduce the fatigue performance of the weld.

4. Conclusions

Rolling after welding has been investigated to determine its influence on distortion and residual stress. The work showed that:

- The friction coefficients between roller and workpiece, and backing-bar and workpiece are important when using high rolling loads. For low loads the frictionless and with friction models produce virtually the same residual stress distribution. In the frictionless models the material deforms more uniformly through the thickness, while in the models with friction the surface constraint imposed by the frictional interaction produces more plastic strain and compressive residual stress in the core of the weld bead. This results in greater tensile stress at the upper surface of the weld.
- Rolling the top of the weld bead reduces residual stress and distortion, and can even result in a compressive residual stress region in the weld bead and surrounding material. The higher the rolling load, the larger the compressive residual stress.
- The modelling results from rolling the top of the weld bead were in very good agreement with the experimental results, in terms of residual stress and out-of-plate distortion reduction.
- The longitudinal residual stress can be reduced by rolling the weldments beside the weld beads. However, the reduction was strongly dependent on the position of the roller with respect to the weld bead, with greater reductions being obtained when the roller “pinched” the weld profile. Therefore, when rolling a weld bead that varies in shape, the residual stress reduction will vary along the length. This rolling method was not as effective in reducing the residual stress in the weld bead, particularly in the middle of the weld and therefore we recommend that rolling on top of the weld bead is the most beneficial technique for weld residual stress and distortion reduction.
- Although the models indicated that rolling the weld toes with the dual flat roller reduced weld distortion, this was not backed up with experiments where there was only a marginal reduction in the distortion compared to the as-welded condition.

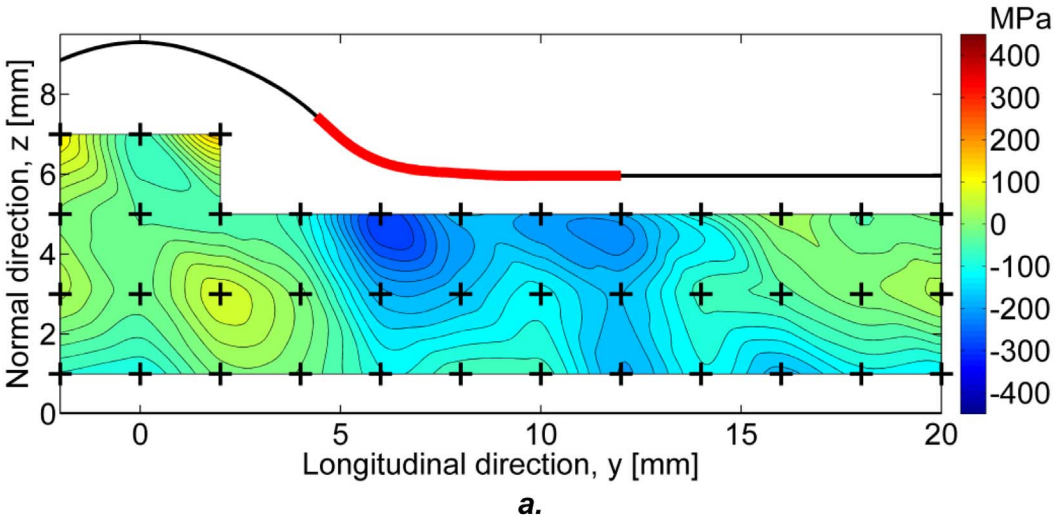

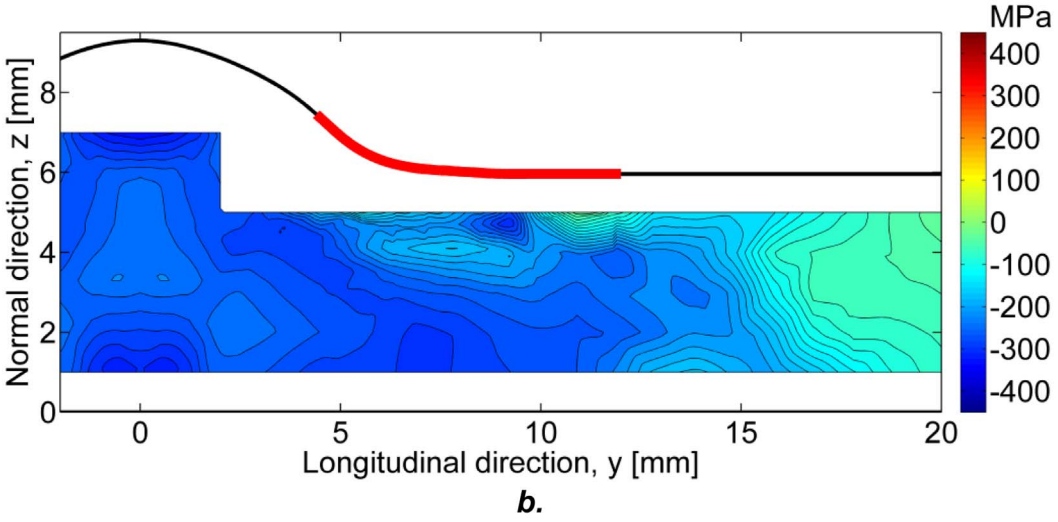

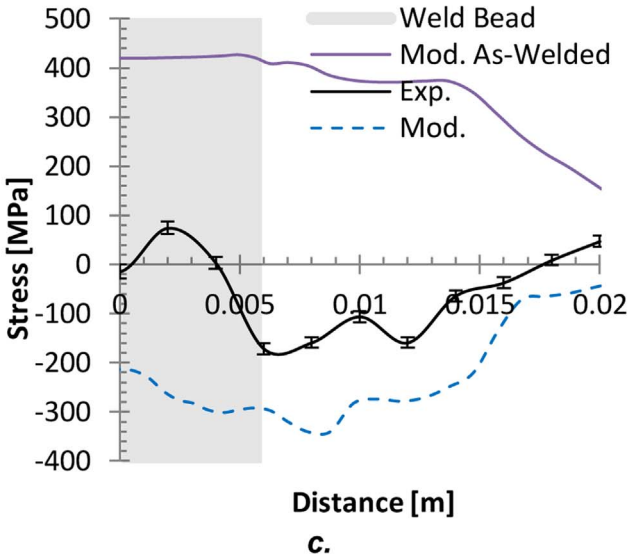

Fig. 16. Contour plot of the longitudinal residual stress after rolling the welding toes, with 150 kn. (a) Experimental (Coules et al., 2013b) and (b) modelling results; and (c) line plot of the centreline showing the comparison between experimental and modelling results. The red line represents the roller contact. (For interpretation of the references to colour in this figure legend, the reader is referred to the web version of this article.)

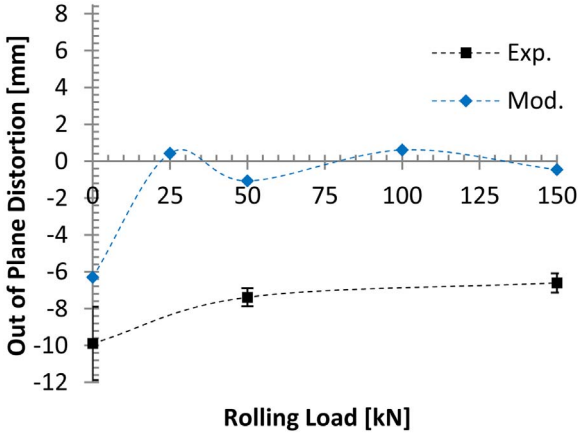

Fig. 17. Peak out-of-plane distortion vs. rolling load, after rolling the weld toes.

Acknowledgements

The authors wish to acknowledge the financial support of EPSRC under grant number EP/G014132/1, and Tata Steel UK. The authors acknowledge beamtime provision from the Institut Laue-Langevin, France, under proposal no. 1-02-68 and the Science and Technology Facilities Council under proposal nos. RB1120159 and RB1210128. The data underpinning this article can be accessed on the Cranfield University data repository, CORD, at https://doi.org/10.17862/cranfield.rd.4834016.

References

Al-Sulaiman, F., Yilbas, B.S., Karatas, C., Keles, O., Uslan, I., Usta, Y., Ahsan, M., Bazoune, A., 2007. Laser cutting of kevlar and mild steel composite structure: end product quality assessment. J. Mater. Eng. Perform. 16, 22–29.

Altenkirch, J., Steuwer, A., Withers, P.J., Williams, S.W., Poad, M., Wen, S.W., 2009. Residual stress engineering in friction stir welds by roller tensioning. Sci. Technol. Weld. Join. 14, 185–192. http://dx.doi.org/10.1179/136217108X388624.

Bijak-Zochowski, M., Marek, P., 1997. Residual stress in some elasto-plastic problems of rolling contact with friction. Int. J. Mech. Sci. 39, 15–32.

Connor, L.P., 1987. Welding Handbook. American Welding Societ, Miami, FL.

Cook, M., Larke, E.C., 1945. Resistance of copper and copper alloys to homogeneous deformation in compression. J. Inst. Met. 71, 371–390.

Coules, H.E., Colegrove, P., Cozzolino, L.D., Wen, S.W., 2012a. Experimental measurement of biaxial thermal stress fields caused by arc welding. J. Mater. Process. Technol. 212, 962–968. http://dx.doi.org/10.1016/j.jmatprotec.2011.12.006.

Coules, H.E., Colegrove, P., Cozzolino, L.D., Wen, S.W., Ganguly, S., Pirling, T., 2012b. Effect of high pressure rolling on weld-induced residual stresses. Sci. Technol. Weld. Join. 17, 394–401. http://dx.doi.org/10.1179/1362171812Y.0000000021.

Coules, H.E., Cozzolino, L.D., Colegrove, P., Ganguly, S., Wen, S.W., Pirling, T., 2012c. Neutron diffraction analysis of complete residual stress tensors in conventional and rolled gas metal arc welds. Exp. Mech. 53 (2), 195–204. http://dx.doi.org/10.1007/s11340-012-9631-3.

Coules, H.E., Colegrove, P., Cozzolino, L.D., Wen, S.W., 2013a. High pressure rolling of low carbon steel weld seams: part 1 − effects on mechanical properties and microstructure. Sci. Technol. Weld. Join. 18, 76–83. http://dx.doi.org/10.1179/1362171812Y.0000000079.

Coules, H.E., Colegrove, P., Cozzolino, L.D., Wen, S.W., Kelleher, J.F., 2013b. High pressure rolling of low carbon steel weld seams: part 2 − roller geometry and residual stress. Sci. Technol. Weld. Join. 18, 84–90. http://dx.doi.org/10.1179/1362171812Y.0000000080.

Coules, H.E., 2012. Characterising the Effects of High-pressure Rolling on Residual Stress in Structural Steel Welds. Cranfield University.

Dessault Systemes, 2009. Abaqus 6.9 documentation. Abaqus Analysis User's Manual.

Goldak, J., Akhlaghi, M., 2005. Computational Welding Mechanics, 1st ed. Springer.

Goldak, J., Chakravarti, A., Bibby, M., 1984. A new finite element model for welding heat sources. Metall. Trans. B 15, 299–305.

Kurkin, S.A., Anufriev, V.I., 1984. Preventing distortion of welded thin-walled members of AMg 6 and 1201 aluminum alloys by rolling the weld with a roller behind the welding arc. Weld. Prod. Engl. Transl. Svarochnoe Proizv. 31, 52–55.

Kurkin, S.A., Tsyao, G., 1962. Reduction of residual stresses in thin-Walled members of titanium alloys. Weld. Prod. Engl. Transl. Svarochnoe Proizv. 10, 1.

Lindgren, L.-E., 2007. Computational Welding Mechanics Thermomechanical and Microstructural Simulations. Woodhead Publishing.

Liu, W., Tian, X., Zhang, X., 1996. Preventing weld hot cracking by synchronous rolling during welding. Weld. J. 75, 297s–304s.

McClung, R.C., 2007. A literature survey on the stability and significance of residual stresses during fatigue. Fatigue Fract. Eng. Mater. Struct. 30, 173–205. http://dx.doi.org/10.1111/j.1460-2695.2007.01102.x.

Michaleris, P., Debiccari, A., 1997. Prediction of welding distortion. Weld. J. (Miami Fla) 76, 172s–180s.

Price, J.W.H., Ziaraparadowska, A., Joshi, S., Finlayson, T., Semetay, C., Nied, H., 2008. Comparison of experimental and theoretical residual stresses in welds: the issue of gauge volume. Int. J. Mech. Sci. 50, 513–521. http://dx.doi.org/10.1016/j.ijmecsci.2007.08.008.

Shan, X.Y., Tan, M.J., O'Dowd, N.P., 2007. Developing a realistic FE analysis method for the welding of a NET single-bead-on-plate test specimen. J. Mater. Process. Technol. 192–193, 497–503. http://dx.doi.org/10.1016/j.jmatprotec.2007.04.080.

Simonson, J.R., 1967. An Introduction to Engineering Heat Transfer, 1st ed. McGRAW-HILL International, London.

Smith, M.C., Smith, A.C., 2009. NeT bead-on-plate round robin: comparison of transient thermal predictions and measurements. Int. J. Press. Vessel. Pip. 86, 96–109. http://dx.doi.org/10.1016/j.ijpvp.2008.11.016.

Thompson, A.M., Fresini, M., Dos Santos, J., Hedgegard, J., Dithey, U., Richardson, I.M., Yapp, D., 2008. Improving the competitiveness of the European steel fabrication industry using synchronised tandem wire welding technology. Mid-term project overview. Luxembourg. http://dx.doi.org/10.2777/1085.

Tryfyakov, V.I., Mikheev, P.P., Kudryavtsev, Y., Paton, E.O., Reznik, D.N., 1993. Ultrasonic impact peening treatment of welds and its effect on fatigue resistance in air and seawater. In: Proceedings of Offshore Technology Conference. The Offshore Technology Conference. Houston, USA. pp. 183–193. http://dx.doi.org/10.4043/7280-MS.

Wen, S.W., Colegrove, P., Williams, S.W., Morgan, S.A., Wescott, A., Poad, M., 2010. Rolling to control residual stress and distortion in friction stir welds. Sci. Technol. Weld. Join. 15, 440–447.

Yang, Y.P., Dong, P., 2011. Buckling distortions and mitigation techniques for thin-section structures. J. Mater. Eng. Perform. 21, 153–160. http://dx.doi.org/10.1007/s11665-011-9928-x.

Yang, Y.P., Dong, P., Tian, X., Zhang, Z., 1998. Prevention of welding hot cracking of high strength aluminum alloys by mechanical rolling. In: Vitek, J.M., David, S.A. (Eds.), ASM Proceedings of the International Conference: Trends in Welding Research. Pine Mountain, GA. pp. 700–705.

2017-04-27

Investigation of post-weld rolling methods to reduce residual stress and distortion

Cozzolino, Luis D.

Elsevier

Luis D. Cozzolino, Harry E. Coules, Paul A. Colegrove, Shuwen Wen, Investigation of post-weld rolling methods to reduce residual stress and distortion, Journal of Materials Processing Technology, Volume 247, September 2017, pp243-256

http://dx.doi.org/10.1016/j.jmatprotec.2017.04.018